PHYSICAL REVIEW D **90,** 014021 (2014)

Effects of $N(2000)5/2^+$, $N(2060)5/2^-$, $N(2120)3/2^-$, and $N(2190)7/2^-$ on $K^*\Lambda$ photoproduction

Sang-Ho Kim,[1,2,*] Atsushi Hosaka,[1,†] and Hyun-Chul Kim[2,3,‡]

[1]*Research Center for Nuclear Physics (RCNP), Osaka 567-0047, Japan*
[2]*Department of Physics, Inha University, Incheon 402-751, Republic of Korea*
[3]*School of Physics, Korea Institute for Advanced Study (KIAS), Seoul 130-722, Republic of Korea*

(Received 7 February 2014; published 14 July 2014)

We reinvestigate $K^*\Lambda(1116)$ photoproduction off the nucleon target, based on an effective Lagrangian approach. We include higher nucleon resonances such as $N(2000)5/2^+$, $N(2060)5/2^-$, $N(2120)3/2^-$, and $N(2190)7/2^-$, of which the data are taken from the 2012 edition of Review of Particle Physics, in addition to the t-channel diagrams (K, K^*, and κ), the s-channel nucleon, and u-channel hyperon (Λ, Σ, and Σ^*) contributions. We find that the $N(2120)3/2^-$ and $N(2190)7/2^-$ resonances are essential in describing the new CLAS Collaboration data for charged K^* photoproduction. On the other hand, they rarely affect neutral K^* photoproduction.

DOI: 10.1103/PhysRevD.90.014021 PACS numbers: 13.60.Le, 14.20.Gk

I. INTRODUCTION

The CLAS Collaboration at the Thomas Jefferson National Accelerator Facility has recently reported the first high-statistics experimental data for both the total and differential cross sections for the reaction $\gamma p \to K^{*+}\Lambda$ [1]. As compared to the previous preliminary data shown in the conference proceedings [2], the total cross section in the resonance region is significantly larger. Though the original motivation of Ref. [1] was to study the role of $\kappa(800)$ mesons involved in the t-channel process, the new CLAS data near the threshold gives us a clue to understanding the role of higher nucleon (N^*) resonances. In a previous work [3], it was found that the N^* resonances indeed played an important role in describing the experimental data near the threshold region. However, the new CLAS data indicates that there are still missing parts in the previous analysis. As discussed in Ref. [1] in detail, all theoretical results [3–6] look different from the CLAS data. In this respect, it is of great importance to reinvestigate the production mechanism of $K^{*+}\Lambda$ photoproduction. In Ref. [3], it was pointed out that certain N^* resonances are essential in describing the former experimental data near the threshold region. In particular, $D_{13}(2080)$ was shown to be crucial in explaining the enhancement of the near-threshold production rate.

In the meanwhile, the data for the N^* resonances in the 2012 edition of Review of Particle Physics [7] were much changed from those in the 2010 edition [8]. This revision is mainly due to a new multichannel partial wave analysis [9]. So far the evidence and properties of N^* resonances were determined by the partial wave analyses of πN scattering data [10], but we are still far from complete understanding. Anisovich *et al*. performed a multichannel partial wave analysis taking both the πN and various photoproduction data [9]. Based on this analysis, a few new N^* resonances were included and some were rearranged in the N^* spectrum [7]. In particular, four new N^* resonances were classified below 1.9 GeV: $N(1860)5/2^+$, $N(1875)3/2^-$, $N(1880)1/2^+$, and $N(1895)1/2^-$ [11,12]. Some of the N^* resonances above the $K^*\Lambda$ threshold were either newly found or rearranged. For example, the mass of the $D_{15}(2200)$ was moved down to $N(2060)5/2^-$ with its photon decay amplitudes added. As for the $N(2190)7/2^-$, its photon decay amplitudes were renewed. A noticeable thing is that the $D_{13}(2080)$ has disappeared in the Particle Data Group (PDG) 2012 edition. Instead, two new resonances with $J^P = 3/2^-$ are included: $N(1875)3/2^-$ and $N(2120)5/2^-$. The old $D_{13}(2080)$ seems to correspond to $N(1875)3/2^-$ below the $K^*\Lambda$ threshold, though the new data of the photon decay helicity amplitudes [7,9] are very different from the old ones [8,13,14]. If one takes this situation seriously, we have to reanalyze the production mechanism of the $\gamma N \to K^*\Lambda$ with the new N^* data employed.

In the present work, we reexamine $K^*\Lambda(1116)$ photoproduction off the nucleon, considering some of the N^* resonances of the PDG 2012 edition above the threshold. We will take $N(2000)5/2^+$, $N(2060)5/2^-$, $N(2120)3/2^-$, and $N(2190)7/2^-$ into account. The last one was omitted in the previous analysis [3] because of the complexity due to its higher spin. The $P_{11}(2100)$ is not included here because of the lack of information. To reduce the ambiguity in determining the coupling constants, we use the experimental data when they are available. As we will show later, the results of the total cross section for the $\gamma p \to K^{*+}\Lambda$ reaction are in remarkable agreement with the new CLAS data [1]. Its differential cross sections are also well reproduced, compared to those from previous works [3–6].

*shkim@rcnp.osaka-u.ac.jp
†hosaka@rcnp.osaka-u.ac.jp
‡hchkim@inha.ac.kr

We predict the total and differential cross sections of the neutral process $\gamma n \to K^{*0}\Lambda$. Anticipating the results from future experiments, we compute the beam, recoil, and target asymmetries of $\gamma N \to K^*\Lambda$ reactions. In addition, we derive some of the double polarization observables.

We sketch the present paper as follows: In Sec. II, we briefly explain the general framework. The effective Lagrangians required for $K^*\Lambda$ photoproduction are presented explicitly. We also describe how to fix the coupling constants and the cutoff masses. In Sec. III, the results of the cross sections are compared with the experimental data for the $\gamma p \to K^*\Lambda$ reaction. We also show the predictions of the polarization observables and discuss them. Section IV is devoted to summary and draws conclusions.

II. FORMALISM

In this section, we briefly explain the general formalism of an effective Lagrangian approach. We refer to Ref. [3] for more details. The tree-level Feynman diagrams relevant to the $\gamma N \to K^*\Lambda$ reaction are shown in Fig. 1; k_1 and p_1 denote, respectively, the momenta of incoming photon and nucleon, while k_2 and p_2 represent those of the outgoing K^* and Λ, respectively. Figure 1(a) stands for the t-channel processes including K^*, K, and κ exchange, Fig. 1(b) shows the s-channel processes containing the nucleon and N^* resonances, Fig. 1(c) corresponds to the u-channel ones with Λ, Σ, and Σ^* exchanges, and Fig. 1(d) is the contact term required to preserve gauge invariance.

The basic forms of the effective Lagrangians were already given in previous works. The photon-meson interactions are described by the following effective Lagrangians:

$$\begin{aligned}
\mathcal{L}_{\gamma K^*K^*} &= -ie_{K^*}A^\mu(K^{*\nu}K^{*\dagger}_{\mu\nu} - K^*_{\mu\nu}K^{*\dagger\nu}),\\
\mathcal{L}_{\gamma K^*K} &= g_{\gamma K^*K}\epsilon^{\mu\nu\alpha\beta}(\partial_\mu A_\nu)(\partial_\alpha K^*_\beta)\bar{K} + \text{H.c.},\\
\mathcal{L}_{\gamma K^*\kappa} &= g_{\gamma K^*\kappa}A^{\mu\nu}\bar{\kappa}K^*_{\mu\nu} + \text{H.c.},
\end{aligned} \tag{1}$$

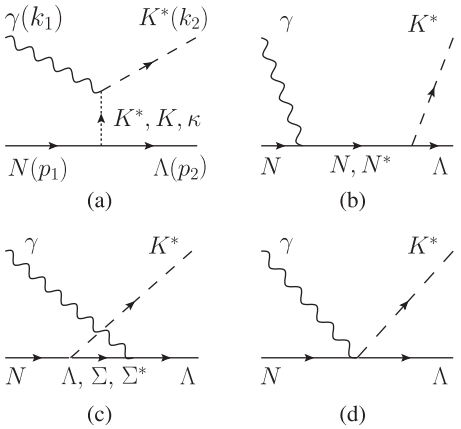

FIG. 1. The tree-level Feynman diagrams for the $\gamma N \to K^*\Lambda$ reaction.

where A_μ, K^*_μ, K, and κ denote the photon, the $K^*(892, 1^-)$ vector meson, the $K(495, 0^-)$ pseudoscalar meson, and the $\kappa(800, 0^+)$ scalar meson, respectively. The $K^*_{\mu\nu}$ represents the field-strength tensor for the K^* vector meson defined as $K^*_{\mu\nu} = \partial_\mu K^*_\nu - \partial_\nu K^*_\mu$. The electric charge of the K^* vector meson is given as e_{K^*}. We take the values of $g_{\gamma K^*K}$ from the experimental data from the PDG [7], which lead to $g^{\text{charged}}_{\gamma K^*K} = 0.254\ \text{GeV}^{-1}$ and $g^{\text{neutral}}_{\gamma K^*K} = -0.388\ \text{GeV}^{-1}$. On the other hand, we utilize the vector-meson dominance [15] to find the values of $g_{\gamma K^*\kappa}$: $g^{\text{charged}}_{\gamma K^*\kappa} = 0.12e\ \text{GeV}^{-1}$ and $g^{\text{neutral}}_{\gamma K^*\kappa} = -0.24e\ \text{GeV}^{-1}$ with the unit electric charge e.

The effective Lagrangians for the electromagnetic (EM) interactions for the baryons are given as

$$\begin{aligned}
\mathcal{L}_{\gamma NN} &= -\bar{N}\left[e_N\gamma_\mu - \frac{e\kappa_N}{2M_N}\sigma_{\mu\nu}\partial^\nu\right]A^\mu N,\\
\mathcal{L}_{\gamma\Lambda\Lambda} &= \frac{e\kappa_\Lambda}{2M_N}\bar{\Lambda}\sigma_{\mu\nu}\partial^\nu A^\mu\Lambda,\\
\mathcal{L}_{\gamma\Lambda\Sigma} &= \frac{e\mu_{\Sigma\Lambda}}{2M_N}\bar{\Sigma}\sigma_{\mu\nu}\partial^\nu A^\mu\Lambda + \text{H.c.},\\
\mathcal{L}_{\gamma\Lambda\Sigma^*} &= -\frac{ie}{2M_N}\left[g^V_{\gamma\Lambda\Sigma^*}\bar{\Lambda}\gamma_\nu - \frac{ig^T_{\gamma\Lambda\Sigma^*}}{2M_N}\partial_\nu\bar{\Lambda}\right]\gamma_5\Sigma^*_\mu F^{\mu\nu} + \text{H.c.},
\end{aligned} \tag{2}$$

where N, Λ, Σ, and Σ^* stand for the nucleon, $\Lambda(1116)$, $\Sigma(1192)$, and $\Sigma^*(1385, 3/2^+)$ hyperon fields, respectively. M_h denotes generically the mass of hadron h. The baryon fields with spin $s = 3/2$ are described by the Rarita-Schwinger field [16,17]. Here, κ_B is the anomalous magnetic moment of a baryon B and $\mu_{\Lambda\Sigma}$ designates the transition magnetic moment between the $\Lambda(1116)$ and the $\Sigma(1192)$. Note that the EM couplings for the spin-3/2 hyperon Σ^* are related to the well-known magnetic dipole ($M1$) and electric quadrupole ($E2$) moments. These coupling constants are determined by the experimental data of the radiative decay width $\Gamma_{\Sigma^*\to\gamma\Lambda}$ [7], which leads to $(g^V_{\gamma\Lambda\Sigma^*}, g^T_{\gamma\Lambda\Sigma^*}) = (3.78, 3.18)$.

The effective Lagrangians for the meson-baryon interactions are

$$\begin{aligned}
\mathcal{L}_{KN\Lambda} &= -ig_{KN\Lambda}\bar{N}\gamma_5\Lambda K + \text{H.c.},\\
\mathcal{L}_{\kappa N\Lambda} &= -g_{\kappa N\Lambda}\bar{N}\Lambda\kappa + \text{H.c.},\\
\mathcal{L}_{K^*NY} &= -g_{K^*NY}\bar{N}\left[\gamma_\mu Y - \frac{\kappa_{K^*NY}}{2M_N}\sigma_{\mu\nu}Y\partial^\nu\right]K^{*\mu} + \text{H.c.},\\
\mathcal{L}_{K^*N\Sigma^*} &= -\frac{if^{(1)}_{K^*N\Sigma^*}}{2M_{K^*}}\bar{K}^*_{\mu\nu}\bar{\Sigma}^{*\mu}\gamma^\nu\gamma_5 N - \frac{f^{(2)}_{K^*N\Sigma^*}}{4M^2_{K^*}}\bar{K}^*_{\mu\nu}\bar{\Sigma}^{*\mu}\gamma_5\partial^\nu N\\
&\quad + \frac{f^{(3)}_{K^*N\Sigma^*}}{4M^2_{K^*}}\partial^\nu\bar{K}^*_{\mu\nu}\bar{\Sigma}^{*\mu}\gamma_5 N + \text{H.c.},
\end{aligned} \tag{3}$$

where $\Sigma = \boldsymbol{\tau}\cdot\Sigma$ and $\Sigma^*_\mu = \boldsymbol{\tau}\cdot\Sigma^*_\mu$. The strong coupling constants are mainly determined by the flavor $SU(3)$ symmetry and hyperon-nucleon potential models (for example, the Nijmegen potential [18]). Considering the Lorentz structure for the vector-meson coupling to the Σ^*, we can write the interaction Lagrangian in terms of the three form factors, which are similar to the case of $\mathcal{L}_{\gamma\Lambda\Sigma^*}$. From the flavor $SU(3)$ symmetry, the value for $f^{(1)}_{K^*N\Sigma^*}$ can be estimated. Because of the lack of experimental and theoretical information on $f^{(2,3)}_{K^*N\Sigma^*}$, we ignore these terms in the present work, which is plausible, since these two coupling constants are smaller than $f^{(1)}_{K^*N\Sigma^*}$. Finally, the contact term should be included only for the charged K^* production to preserve the $U(1)$ gauge invariance. The corresponding Lagrangian is written as

$$\mathcal{L}_{\gamma K^*N\Lambda} = -\frac{ie_{K^*}g_{K^*N\Lambda}\kappa_{K^*N\Lambda}}{2M_N}\bar{\Lambda}\sigma^{\mu\nu}A_\nu K^*_\mu N + \text{H.c.} \quad (4)$$

As for the details of the relevant coupling constants and other parameters, we refer to Ref. [3].

In addition to the effective Lagrangians for the basic processes discussed above, we now consider those for the N^* resonances. The EM Lagrangians for the N^* resonances from spin $1/2$ to $7/2$ are given as

$$\begin{aligned}
\mathcal{L}_{\gamma NN^*}\left(\frac{1}{2}\right)^\pm &= \frac{eh_1}{2M_N}\bar{N}\Gamma^{(\mp)}\sigma_{\mu\nu}\partial^\nu A^\mu N^* + \text{H.c.},\\
\mathcal{L}_{\gamma NN^*}\left(\frac{3}{2}\right)^\pm &= -ie\left[\frac{h_1}{2M_N}\bar{N}\Gamma^{(\pm)}_\nu - \frac{ih_2}{(2M_N)^2}\partial_\nu\bar{N}\Gamma^{(\pm)}\right]\\
&\quad\times F^{\mu\nu}N^*_\mu + \text{H.c.},\\
\mathcal{L}_{\gamma NN^*}\left(\frac{5}{2}\right)^\pm &= e\left[\frac{h_1}{(2M_N)^2}\bar{N}\Gamma^{(\mp)}_\nu - \frac{ih_2}{(2M_N)^3}\partial_\nu\bar{N}\Gamma^{(\mp)}\right]\\
&\quad\times \partial^\alpha F^{\mu\nu}N^*_{\mu\alpha} + \text{H.c.},\\
\mathcal{L}_{\gamma NN^*}\left(\frac{7}{2}\right)^\pm &= ie\left[\frac{h_1}{(2M_N)^3}\bar{N}\Gamma^{(\pm)}_\nu - \frac{ih_2}{(2M_N)^4}\partial_\nu\bar{N}\Gamma^{(\pm)}\right]\\
&\quad\times \partial^\alpha\partial^\beta F^{\mu\nu}N^*_{\mu\alpha\beta} + \text{H.c.},
\end{aligned} \quad (5)$$

where N^* denotes the corresponding nucleon resonance field. The $\Gamma^{(\pm)}$ and the $\Gamma^{(\pm)}_\mu$ are defined, respectively, as

$$\Gamma^{(\pm)} = \begin{pmatrix}\gamma_5\\ \mathbf{1}\end{pmatrix}, \qquad \Gamma^{(\pm)}_\mu = \begin{pmatrix}\gamma_\mu\gamma_5\\ \gamma_\mu\end{pmatrix}. \quad (6)$$

The effective Lagrangians for the strong vertices including the N^* resonances are expressed as

$$\begin{aligned}
\mathcal{L}_{K^*\Lambda N^*}\left(\frac{1}{2}\right)^\pm &= -\frac{1}{2M_N}\bar{N}^*\left[g_1\left(\pm\frac{\Gamma^{(\mp)}_\mu\Lambda\partial^2}{M_R\mp M_N} - i\Gamma^{(\mp)}\partial_\mu\right) - g_2\Gamma^{(\mp)}\sigma_{\mu\nu}\Lambda\partial^\nu\right]K^{*\mu} + \text{H.c.},\\
\mathcal{L}_{K^*\Lambda N^*}\left(\frac{3}{2}\right)^\pm &= i\bar{N}^*_\mu\left[\frac{g_1}{2M_N}\Lambda\Gamma^{(\pm)}_\nu \mp \frac{ig_2}{(2M_N)^2}\partial_\nu\Lambda\Gamma^{(\pm)} \pm \frac{ig_3}{(2M_N)^2}\Lambda\Gamma^{(\pm)}\partial_\nu\right]K^{*\mu\nu} + \text{H.c.},\\
\mathcal{L}_{K^*\Lambda N^*}\left(\frac{5}{2}\right)^\pm &= \bar{N}^*_{\mu\alpha}\left[\frac{g_1}{(2M_N)^2}\Lambda\Gamma^{(\mp)}_\nu \pm \frac{ig_2}{(2M_N)^3}\partial_\nu\Lambda\Gamma^{(\mp)} \mp \frac{ig_3}{(2M_N)^3}\Lambda\Gamma^{(\mp)}\partial_\nu\right]\partial^\alpha K^{*\mu\nu} + \text{H.c.},\\
\mathcal{L}_{K^*\Lambda N^*}\left(\frac{7}{2}\right)^\pm &= -i\bar{N}^*_{\mu\alpha\beta}\left[\frac{g_1}{(2M_N)^3}\Lambda\Gamma^{(\pm)}_\nu \mp \frac{ig_2}{(2M_N)^4}\partial_\nu\Lambda\Gamma^{(\pm)} \pm \frac{ig_3}{(2M_N)^4}\Lambda\Gamma^{(\pm)}\partial_\nu\right]\partial^\alpha\partial^\beta K^{*\mu\nu} + \text{H.c.}
\end{aligned} \quad (7)$$

The N^* resonance field for a spin of $3/2$ is treated as the Rarita-Schwinger field [16,17], so that the corresponding propagator with momentum p and mass M is written as

$$\Delta_{\alpha\beta}(p,M) = \frac{i(\not{p}+M)}{p^2-M^2}\left[-g_{\alpha\beta} + \frac{1}{3}\gamma_\alpha\gamma_\beta + \frac{1}{3M}(\gamma_\alpha p_\beta - \gamma_\beta p_\alpha) + \frac{2}{3M^2}p_\alpha p_\beta\right]. \quad (8)$$

The propagators of the N^* resonance fields for spins of $5/2$ and $7/2$ are expressed [19–22] as

$$\begin{aligned}
\Delta_{\alpha_1\alpha_2;\beta_1\beta_2}(p,M) &= \frac{i(\not{p}+M)}{p^2-M^2}\\
&\quad\times\left[\frac{1}{2}(\bar{g}_{\alpha_1\beta_1}\bar{g}_{\alpha_2\beta_2}+\bar{g}_{\alpha_1\beta_2}\bar{g}_{\alpha_2\beta_1}) - \frac{1}{5}\bar{g}_{\alpha_1\alpha_2}\bar{g}_{\beta_1\beta_2} - \frac{1}{10}(\bar{\gamma}_{\alpha_1}\bar{\gamma}_{\beta_1}\bar{g}_{\alpha_2\beta_2}+\bar{\gamma}_{\alpha_1}\bar{\gamma}_{\beta_2}\bar{g}_{\alpha_2\beta_1}+\bar{\gamma}_{\alpha_2}\bar{\gamma}_{\beta_1}\bar{g}_{\alpha_1\beta_2}+\bar{\gamma}_{\alpha_2}\bar{\gamma}_{\beta_2}\bar{g}_{\alpha_1\beta_1})\right],\\
\Delta_{\alpha_1\alpha_2\alpha_3;\beta_1\beta_2\beta_3}(p,M) &= \frac{i(\not{p}+M)}{p^2-M^2}\frac{1}{36}\sum_{P(\alpha),P(\beta)}\left[-\bar{g}_{\alpha_1\beta_1}\bar{g}_{\alpha_2\beta_2}\bar{g}_{\alpha_3\beta_3} + \frac{3}{7}\bar{g}_{\alpha_1\beta_1}\bar{g}_{\alpha_2\alpha_3}\bar{g}_{\beta_2\beta_3} + \frac{3}{7}\bar{\gamma}_{\alpha_1}\bar{\gamma}_{\beta_1}\bar{g}_{\alpha_2\beta_2}\bar{g}_{\alpha_3\beta_3} - \frac{3}{35}\bar{\gamma}_{\alpha_1}\bar{\gamma}_{\beta_1}\bar{g}_{\alpha_2\alpha_3}\bar{g}_{\beta_2\beta_3}\right],
\end{aligned} \quad (9)$$

TABLE I. The masses, the decay widths, and the relevant parameters for the N^* resonances. The helicity amplitudes $A_{1,3}$ [10^{-3} GeV$^{-\frac{1}{2}}$] are obtained from Refs. [9,24,25] and the decay amplitudes $G(l,s)$ [GeV$^{\frac{1}{2}}$] are estimated from Ref. [26]. Those in parentheses correspond to the neutron resonances.

PDG	M_{BW}	Γ_{BW}	A_1	A_3	h_1	h_2	$G(l,s)$	g_1	g_1(final)
$N(2000)5/2^+$	2090	460	+32(−18)	+48(−35)	+0.114(−0.395)	+1.22(−0.500)	+0.3	+1.37	+1.37
$N(2060)5/2^-$	2060	375	+67(+25)	+55(−37)	−2.45(+0.027)	−3.81(−2.85)	+0.2	+5.42	+5.42
$N(2120)3/2^-$	2150	330	+130(+110)	+150(+40)	−0.827(−1.66)	+2.14(+2.31)	+3.8	+1.29	+0.30
$N(2190)7/2^-$	2180	335	−34(+10)	+28(−14)	+7.87(−2.94)	−7.36(+2.49)	+2.5	−44.3	−44.3

where the sum is over all permutations of α's and β's and

$$\bar{g}_{\alpha\beta} = g_{\alpha\beta} - \frac{p_\alpha p_\beta}{M^2}, \qquad \bar{\gamma}_\alpha = \gamma_\alpha - \frac{p_\alpha}{M^2}\not{p}. \tag{10}$$

Here, the mass of the N^* resonance in the N^* propagator is replaced as $M \to M - i\Gamma/2$ with its decay width Γ. In general, off-shell parameters may appear in resonance propagators and vertices. However, such off-shell effects are not significant because resonances come into play near the on-mass shell region [23], which has been verified numerically.

We employ the data for the N^* resonances taken from the PDG 2012 edition [7], as mentioned in detail in the Introduction. We consider in this work $N(2000)5/2^+$, $N(2060)5/2^-$, $N(2120)3/2^-$, and $N(2190)7/2^-$ near the threshold region. The values of the masses and decay widths are taken from the Breit-Wigner values [9,24]. The transition magnetic moments h_1 and h_2 given in Eq. (5) are determined by the Breit-Wigner helicity amplitudes taken from Refs. [9,24] or by the predictions from the relativistic quark model [25]: the parameters for $N(2000)5/2^+$, $N(2060)5/2^-$, and $N(2120)3/2^-$ are taken from Refs. [9,24], whereas those for $N(2190)7/2^-$ are determined by using the results in Ref. [25].

The strong coupling constants in Eq. (7), g_i, are found by the following relation,

$$\Gamma_{N^*\to K^*\Lambda} = \sum_{l,s} |G(l,s)|^2, \tag{11}$$

where the explicit form of the decay amplitudes $G(l,s)$ is given in Ref. [26]. Here, we take into account the lowest partial wave contribution for $G(l,s)$ and therefore only the lowest multipole—i.e., the first term of Eq. (7)—is considered, as in Ref. [3]. This assumption is reasonable, as will be shown in the next section. The signs of these strong coupling constants are determined phenomenologically. Because of a lack of information, we also assume that $N(2000)5/2^+$, $N(2060)5/2^-$, $N(2120)3/2^-$, and $N(2190)7/2^-$ may correspond respectively to $F_{15}(2000)$, $D_{15}(2200)$, $D_{13}(2080)$, and $G_{17}(2190)$ in the PDG 2010 edition [8]. However, as will be discussed in the next section, the $N(2120)3/2^-$ turns out to be distinguished from the old $D_{13}(2080)$ that played an important role in the previous work [3]. In fact, the $D_{13}(2080)$ more or less corresponds to the lower-lying three-star N^* resonance $N(1875)3/2^-$. Thus, we have to fit the parameters of the $N(2120)3/2^-$ to the experimental data. Table I lists the relevant parameters for the N^* resonances used in this work.

Using the Lagrangians for the various vertices, we can obtain the scattering amplitudes of t, s, and u channels and contact terms, where the s channel includes N^* resonances. Furthermore, for the K^*, κ, and Σ^* exchanges, we take into account the decay widths in their propagators, 50.8, 550, and 36 MeV, respectively [7].

In an effective Lagrangian approach, it is essential to consider a form factor at each vertex, since it parametrizes the structure of the hadron. However, it is in fact rather difficult to handle the form factors at an EM vertex since it is well known that it breaks the gauge invariance due to its nonlocality [27]. To circumvent this problem, we follow a prescription explained in Refs. [28–30]. Though it is phenomenological, it provides a convenient way of handling the form factors for an EM vertex. The form factors for off-shell mesons and baryons are given, respectively, as

$$F_\Phi = \frac{\Lambda_\Phi^2 - M_\Phi^2}{\Lambda_\Phi^2 - p^2}, \qquad F_B = \frac{\Lambda_B^4}{\Lambda_B^4 + (p^2 - M_B^2)^2}, \tag{12}$$

where $M_{(\Phi,B)}$ and p denote the mass and the momentum of the off-shell hadron, respectively. In order to preserve gauge invariance for the charged K^* production, we consider a common form factor for K^* and N exchanges as

$$F_{\rm com} = F_{K^*}F_N - F_{K^*} - F_N. \tag{13}$$

The neutral K^* production does not require this. The cutoff parameters are determined phenomenologically. However, to reduce theoretical ambiguities due to the wide range of the cutoff values, we limit their values to around 1 GeV.

III. RESULTS AND DISCUSSION

Before we start the detailed discussions for the present results in comparison with the new data, we would like to briefly summarize the current and past situations of the experimental and theoretical studies for the $\gamma p \to K^{*+}\Lambda$ reaction. Before the new CLAS data was announced in Ref. [1], there were two preliminary data that were already reported in Refs. [2,31]. In Ref. [2], only the preliminary

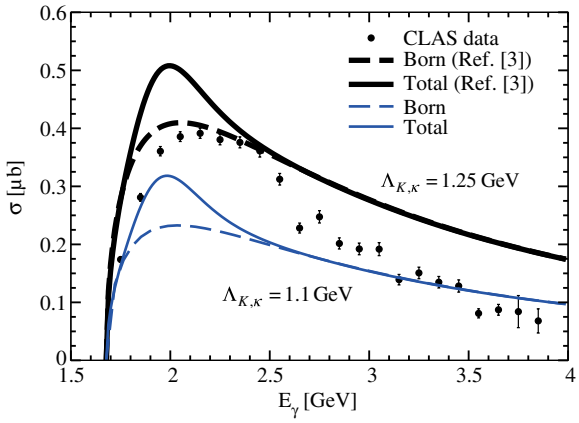

FIG. 2 (color online). Total cross sections when using $\Lambda_{K,\kappa} = 1.25$ GeV (thicker curves) and 1.1 GeV (thinner ones). The dashed curves are the results only with the Born terms, and the solid ones for the inclusion of resonances of Ref. [3].

total cross sections were shown, while in Ref. [31] only the differential cross sections were presented. Using those preliminary data, the previous theoretical studies were done [3,4]. Now in the new CLAS data, both the total and differential cross sections are given.

One of the differences between Ref. [3] and Ref. [4] is the choice of the cutoff values for the K and κ exchanges in the t channel, which are $\Lambda_{K,\kappa} = 1.25$ GeV and $\Lambda_{K,\kappa} = 1.1$ GeV, respectively, to reproduce the used experimental data. Another difference is that in Ref. [3], resonances are included, while in Ref. [4] they are not. Now using the new data, it turns out that the cutoff $\Lambda_{K,\kappa}$ should be taken at around 1.1 GeV. In Fig. 2, we show total cross sections when using $\Lambda_{K,\kappa} = 1.25$ GeV (thicker curves) and 1.1 GeV (thinner ones).

As we can see from this figure, the result of $\Lambda_{K,\kappa} = 1.25$ GeV overestimates the total cross section. The one of $\Lambda_{K,\kappa} = 1.1$ GeV agrees better, especially at higher energies. The discrepancy near the threshold region is improved by the nucleon resonances, but not enough to describe the experimental data, which is the issue of the present paper.

Now in Fig. 3, we show the new results for the total cross section with various contributions. In the left panel, the total cross section with the background contribution and with the total contributions of all the N^* resonances are shown. The dashed curve includes the Born diagrams presented in Fig. 1 without the N^* resonances. The result more or less corresponds to that of Ref. [4]. The dotted one depicts the contribution of the N^* resonances. The cutoff parameters are set as $\Lambda_{K^*,N,\Lambda,\Sigma,\Sigma^*} = 0.9$ GeV, $\Lambda_{K,\kappa} = 1.1$ GeV, and $\Lambda_R = 1.0$ GeV. With the inclusion of the N^* resonances, the present theoretical result is drawn as the solid curve, which describes the experimental data very well.

Let us discuss the details of resonance contributions as shown in the right panel of Fig. 3. The contribution from $N(2000)5/2^+$ turns out to be almost negligible. The $N(2060)5/2^-$ makes a small contribution to the total cross section. Concerning $N(2120)3/2^-$, we first assume that it corresponds to the old $D_{13}(2080)$ since their masses are similar to each other with the same spin quantum numbers. As done in Ref. [3], we have computed the effect of $N(2120)3/2^-$ but it turns out to be overestimated in comparison with the experimental data. In fact, it has yielded approximately ~ 1.9 μb for the total cross section. Thus, we determine the strong coupling constant of $N(2120)3/2^-$ by fitting it to the data for the total cross section. As a result, the coupling constant g_1 is changed from $+1.29$ to $+0.30$, as shown in Table I. Bearing in mind this fact, we show in the right panel of Fig. 3 that the $N(2120)3/2^-$ makes an important contribution to the total cross section, with a peak of around 2 GeV. The $N(2190)7/2^-$ also turns out to be equally as important as $N(2120)3/2^-$. In particular, it governs the dependence

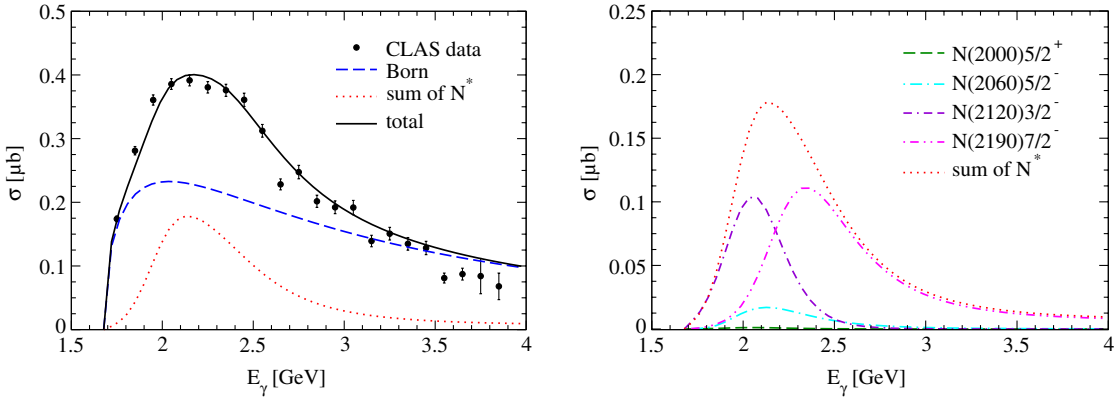

FIG. 3 (color online). The results of the total cross sections for the $\gamma p \to K^{*+}\Lambda$ reaction in the left panel. The dashed curve includes the Born diagrams presented in Fig. 1 without the N^* resonances. The dotted curve shows the contribution of the N^* resonances. The solid curve draws the total contribution of all diagrams. The black circles denote the new CLAS data [1]. The right panel illustrates each contribution of the N^* resonances.

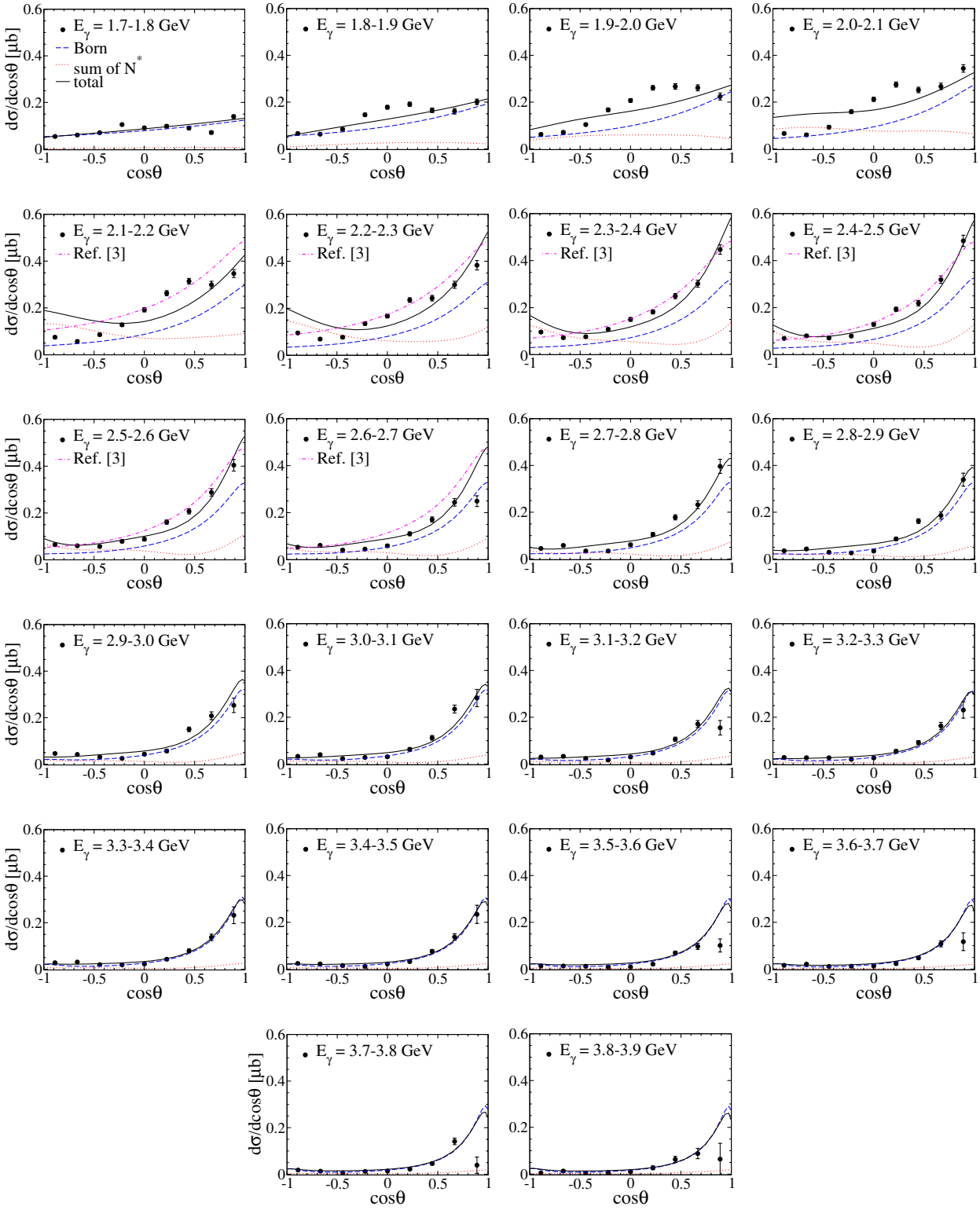

FIG. 4 (color online). Differential cross sections for the $\gamma p \to K^{*+}\Lambda$ reaction as a function of $\cos\theta$ in the range of 1.7 GeV $\leq E_\gamma \leq$ 3.9 GeV. The notations are the same as in the left panel of Fig. 3.

of the total cross section on the photon energy E_γ in higher E_γ regions. With these two N^* resonances taken into account, the experimental data for the total cross section are well reproduced.

In Fig. 4, the differential cross sections are plotted as a function of $\cos\theta$ in the range of 1.7 GeV $\leq E_\gamma \leq$ 3.9 GeV. The effects of the N^* resonances seem to be negligible in the vicinity of the threshold energy, as shown in the first

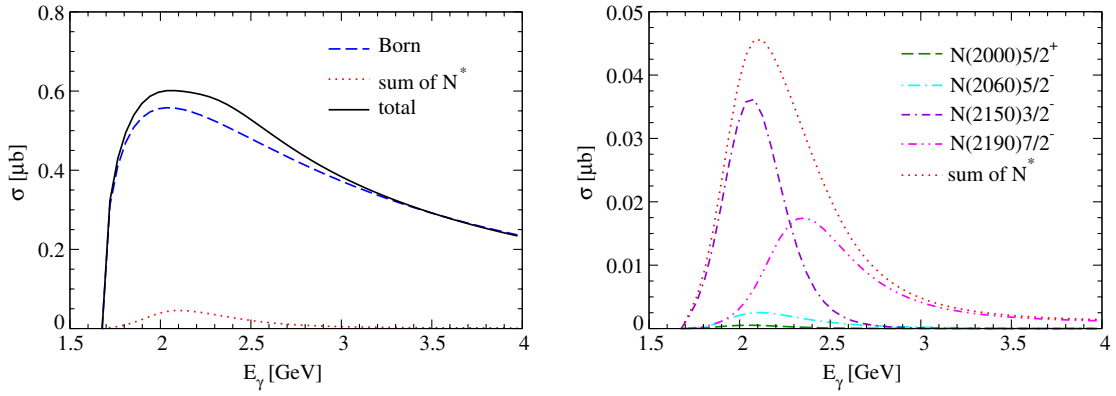

FIG. 5 (color online). The results of the total cross sections for the $\gamma n \to K^{*0}\Lambda$ reaction in the left panel. The solid curve draws the total contribution of all diagrams, whereas the dashed one shows that of the Born terms except for the N^* resonances. The dotted curve depicts the contribution of the N^* resonances to the total cross section. The right panel illustrates each contribution of the N^* resonances.

panel of Fig. 4. However, as the photon energy increases, the N^* resonances come into play. Apart from the structures of a broad bump in the experimental data in the range 1.8 GeV $\leq E_\gamma \leq$ 2.3 GeV, the present results are in good agreement with the data in general. Experimentally, the differential cross sections in the forward direction start to increase as E_γ does. This feature is qualitatively explained by the Born terms but can be described quantitatively only by including the N^* resonances. The experimental data in the forward direction remain almost constant with little energy dependence in the range of 3.2 GeV $\leq E_\gamma \leq$ 3.5 GeV, then start to fall off drastically above 3.5 GeV. The present model is not able to describe this behavior of the data. Considering the fact that the present approach of effective Lagrangians is built for lower E_γ regions, one has to take into account more degrees of freedom or a more sophisticated theoretical method to explain the $\gamma p \to K^{*+}\Lambda$ at higher photon energies. On the other hand, as shown in some energy range, i.e., 2.1 GeV $\leq E_\gamma \leq$ 2.6 GeV, we find with the main contribution of $D_{13}(2080)$ [3] that the theoretical calculations slightly overestimate the CLAS data, which is expected from Fig. 2. We want to mention that the role of the N^* resonances for the $\gamma N \to K^*\Lambda$ reaction look very different from that for $\gamma p \to K^*\Sigma$, where the N^* resonances are almost negligible. We refer to Refs. [32,33] for details.

In the left panel of Fig. 5, we predict the total cross section for the $\gamma n \to K^{*0}\Lambda$ reaction. The neutral charge of the K^{*0} makes the K^* exchange and the contact term absent in this reaction. Nevertheless, the magnitude of this total cross section is quite a bit larger than that of the charged process $\gamma p \to K^{*+}\Lambda$ because of the large neutral coupling constant of the $\gamma K K^*$ interaction, as discussed in detail in Ref. [3]. Thus, the main contribution to the total cross section for the $\gamma n \to K^{*0}\Lambda$ reaction arises from the K exchange. Moreover, the effects of the N^* resonances are almost marginal for the neutral process. Each contribution of the four N^* resonances drawn is illustrated in the right panel of Fig. 5. Figure 6 depicts the differential cross section as a function of $\cos\theta$ with E_γ varied from 1.9 GeV to 2.7 GeV. The experimental data for the $\gamma n \to K^{*0}\Lambda$ reaction will soon appear.

We now want to discuss the polarization observables [34–36], which provide crucial information on the helicity amplitudes and spin structure of a process. To define the polarization observables, the reaction takes place in the $x-z$ plane with the photon beam. We first start with the single polarization observables. Since we also consider the double polarization observables, we will follow the notation for the polarized differential cross sections defined in Ref. [36]:

$$d\sigma(B,T;R,V) = \frac{d\sigma}{d\Omega}(B,T;R,V), \tag{14}$$

where B, T, R, and V denote the polarizations of the photon beam (B), the target nucleon (T), the recoil Λ (R), and the produced K^* vector meson (V), respectively, involved in the $\gamma N \to K^*\Lambda$ process. According to the notation defined in Eq. (14), we define the photon-beam asymmetry (Σ_x), the target asymmetry (T_y), and the recoil asymmetry (P_y) as

$$\begin{aligned}
\Sigma_x &= \frac{d\sigma(\perp,U;U,U) - d\sigma(\parallel,U;U,U)}{d\sigma(\perp,U;U,U) + d\sigma(\parallel,U;U,U)},\\
T_y &= \frac{d\sigma(U,y;U,U) - d\sigma(U,-y;U,U)}{d\sigma(U,y;U,U) + d\sigma(U,-y;U,U)},\\
P_y &= \frac{d\sigma(U,U;y,U) - d\sigma(U,U;-y,U)}{d\sigma(U,U;y,U) + d\sigma(U,U;-y,U)},
\end{aligned} \tag{15}$$

where $\parallel$ and $\perp$ denote the linear polarizations of the photon along the direction of the $\boldsymbol{x}$ and $\boldsymbol{y}$ axes, respectively; y and $-y$ represent the polarization states of the N (Λ), which lie in the direction of the $\boldsymbol{y}$ and $-\boldsymbol{y}$ axes, respectively. The U means that the corresponding particle state is unpolarized. These three asymmetries satisfy the following collinear condition:

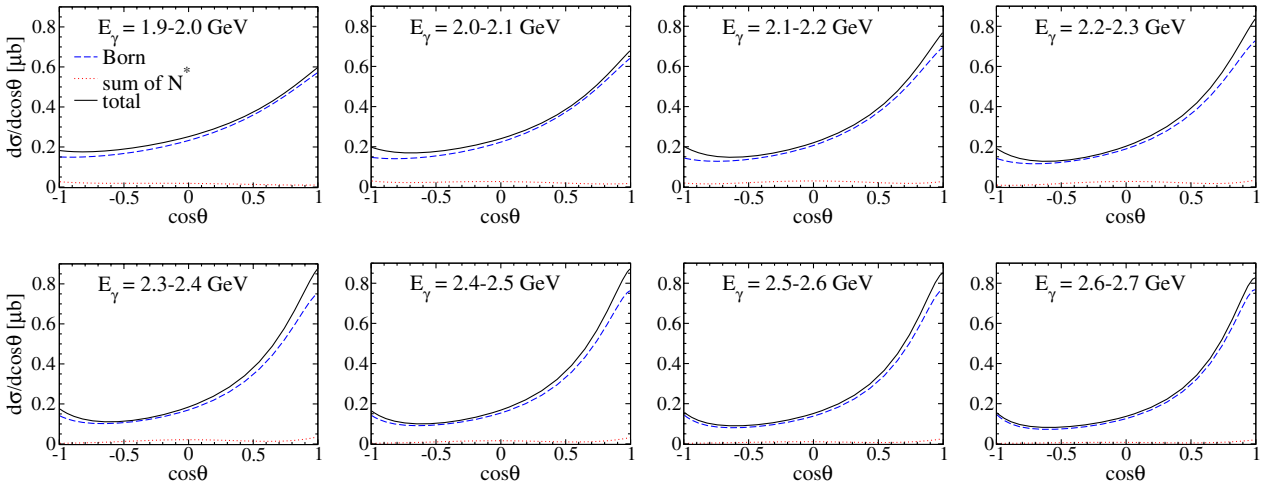

FIG. 6 (color online). Differential cross sections for the $\gamma n \to K^{*0}\Lambda$ reaction as a function of $\cos\theta$ in the range of 1.9 GeV $\leq E_\gamma \leq$ 2.7 GeV. The notations are the same as in the left panel of Fig. 5.

$$\Sigma_x = T_y = P_y = 0 \quad \text{at} \quad \cos\theta = \pm 1. \tag{16}$$

The upper panel of Fig. 7 depicts the results of the photon-beam asymmetries for the charged process $\gamma p \to K^{*+}\Lambda$ at two different photon energies, $E_\gamma = 2.15$ GeV and $E_\gamma = 2.65$ GeV. As was already discussed in Ref. [3], the beam asymmetry is almost compatible with zero without the N^* resonances. Including them, we find that Σ_x becomes positive and has broad bump structures. Thus, the measurement of the beam symmetry can already tell whether the N^* resonances are indeed important in understanding the production mechanism of the $\gamma p \to K^{*+}\Lambda$ reaction. In the lower panel of Fig. 7, we draw the results of the Σ_x for the neutral $\gamma n \to K^{*0}\Lambda$ reaction. It is interesting to see that the effects of the N^* resonances turn out to be rather small in this case. We already saw that their contribution to the total and differential cross sections are marginal since the contribution of the K meson exchange governs the $\gamma n \to K^{*0}\Lambda$ reaction. By the same token, the effects of the N^* resonances seem to be suppressed in the beam asymmetries for the neutral process.

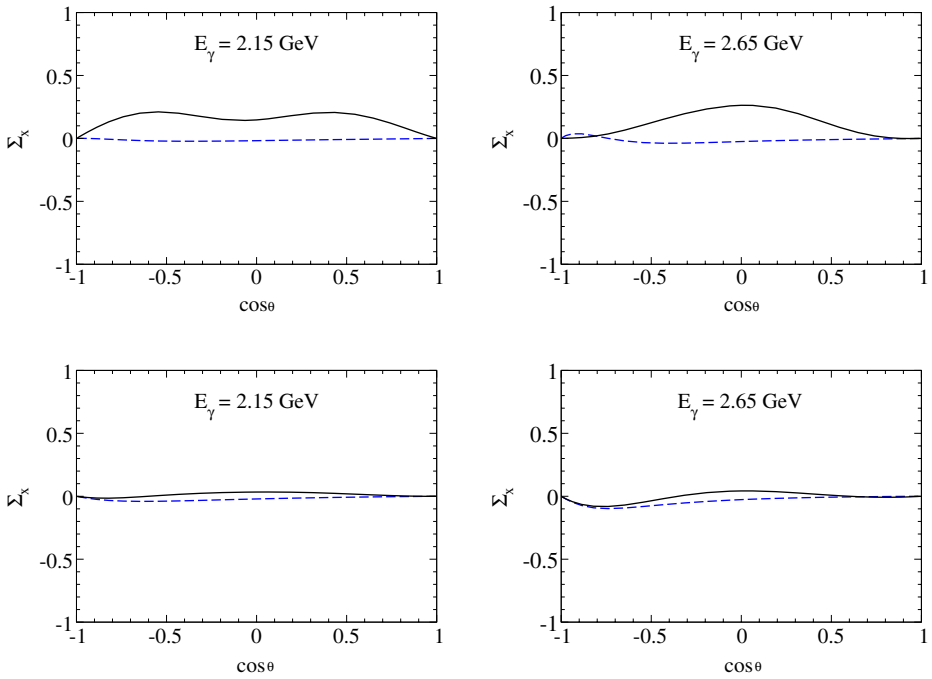

FIG. 7 (color online). The photon-beam asymmetries as functions of $\cos\theta$ with two different photon energies, $E_\gamma = 2.15$ GeV and $E_\gamma = 2.65$ GeV. In the upper panel, we draw the Σ_x for the $\gamma p \to K^{*+}\Lambda$ reaction, while in the lower panel we do so for the $\gamma n \to K^{*0}\Lambda$ reaction. The solid curves represent the total results including the N^* resonances, whereas the dashed ones show those without them.

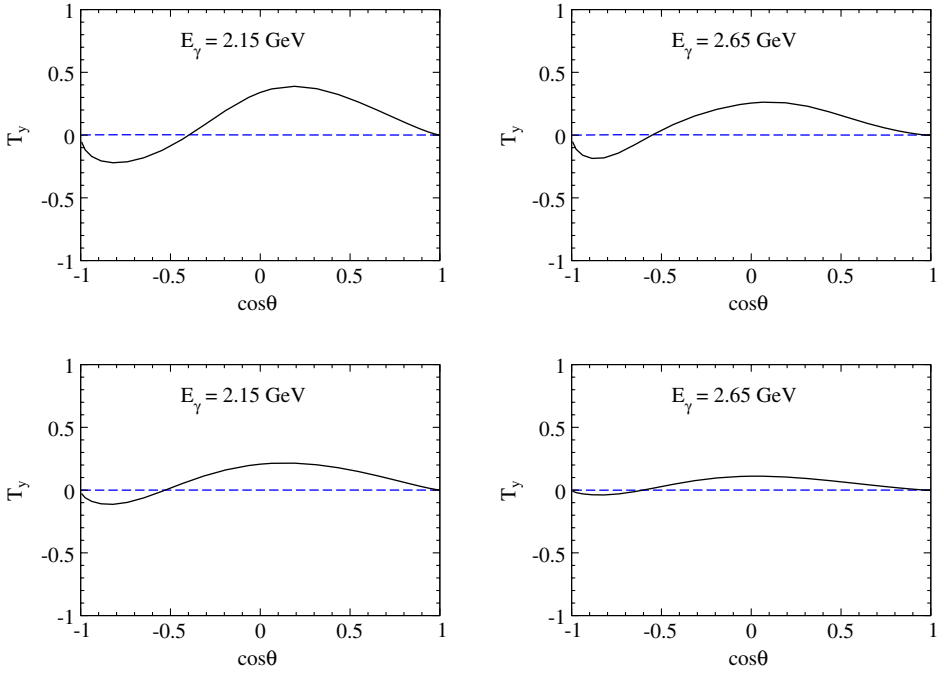

FIG. 8 (color online). The target asymmetries as functions of $\cos\theta$ with two different photon energies, $E_\gamma = 2.15$ GeV and $E_\gamma = 2.65$ GeV. In the upper panel, we draw the T_y for the $\gamma p \to K^{*+}\Lambda$ reaction, while in the lower panel we do so for the $\gamma n \to K^{*0}\Lambda$ reaction. Notations are the same as in Fig. 7.

In Figs. 8 and 9, the results of the target and recoil asymmetries are drawn, respectively. As in Fig. 7, the upper panel is for the $\gamma p \to K^{*+}\Lambda$ reaction and the lower panel corresponds to the $\gamma n \to K^{*0}\Lambda$ reaction. The dependence of the T_y on $\cos\theta$ is distinguished from that of the beam asymmetry. The values of the T_y become positive from the very forward angle till the backward angle and then turn negative around $\cos\theta = -0.5(\theta = 120^\circ)$. In the case of the

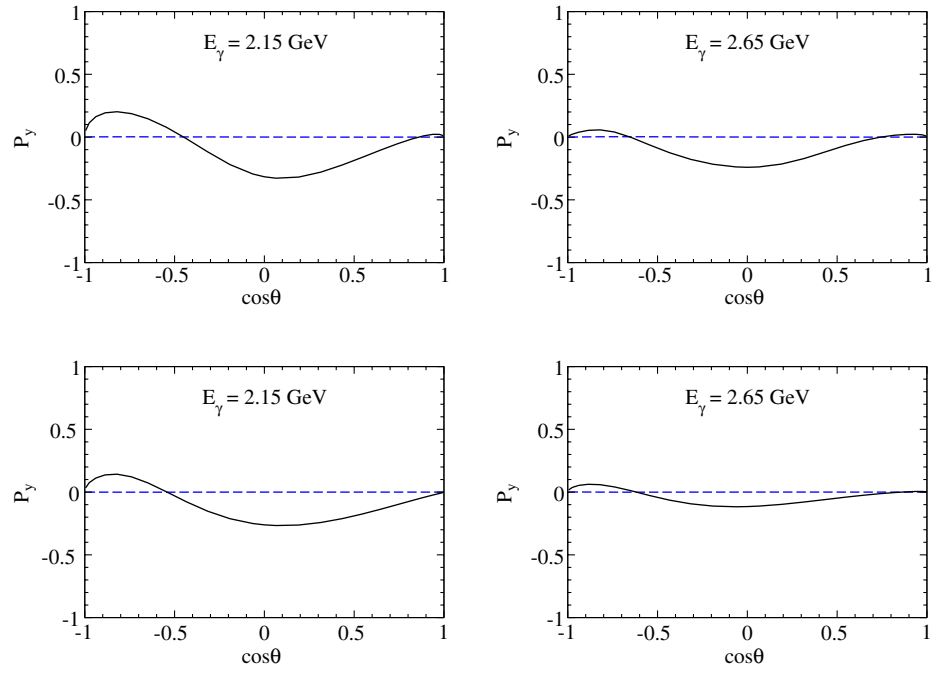

FIG. 9 (color online). The recoil asymmetries as functions of $\cos\theta$ with two different photon energies, $E_\gamma = 2.15$ GeV and $E_\gamma = 2.65$ GeV. In the upper panel, we draw the P_y for the $\gamma p \to K^{*+}\Lambda$ reaction, while in the lower panel we do so for the $\gamma n \to K^{*0}\Lambda$ reaction. Notations are the same as in Fig. 7.

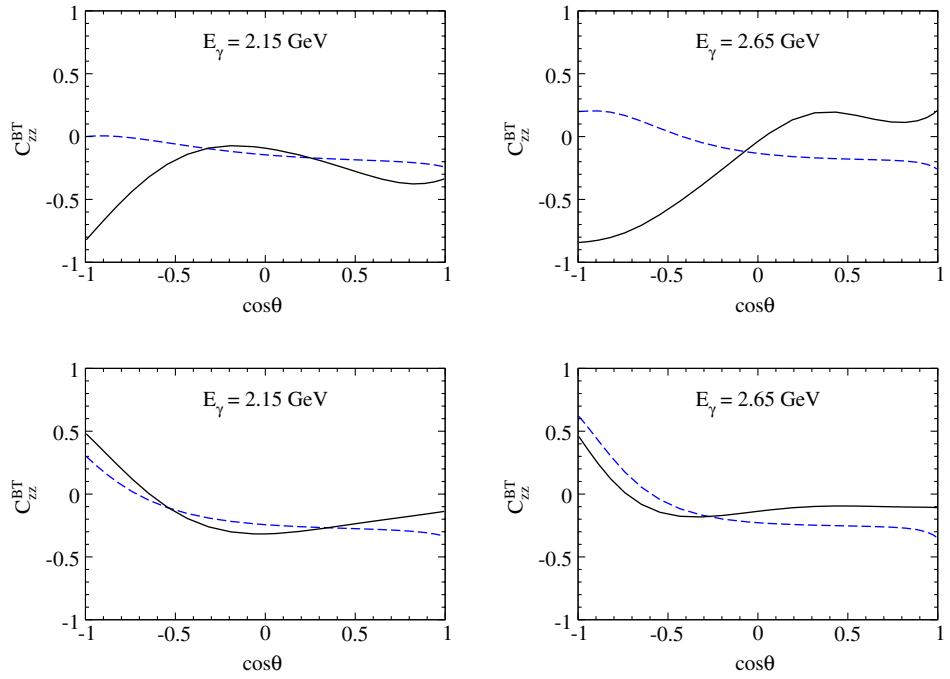

FIG. 10 (color online). The beam-target asymmetries as functions of $\cos\theta$ with two different photon energies, $E_\gamma = 2.15$ GeV and $E_\gamma = 2.65$ GeV. In the upper panel, we draw the C_{zz}^{BT} for the $\gamma p \to K^{*+}\Lambda$ reaction, while in the lower panel we do so for the $\gamma n \to K^{*0}\Lambda$ reaction. Notations are the same as in Fig. 7.

recoil asymmetries, the results are just the opposite of those of the target asymmetries. Both the target and recoil asymmetries become smaller in magnitude as the photon energy increases, while the form of the dependence on the scattering angle is kept. As found in the results of the differential cross sections, the N^* resonances mainly explain the production mechanism in the vicinity of the threshold energy. This can be seen also in the single spin polarization observables.

We now discuss the double polarization asymmetries. In fact, there are many different polarization observables in the vector meson photoproduction. Here, we will consider only some of the double polarization asymmetries, which are defined as follows:

$$
\begin{aligned}
C_{zz}^{\mathrm{BT}} &= \frac{d\sigma(r,z;U,U) - d\sigma(r,-z;U,U)}{d\sigma(r,z;U,U) + d\sigma(r,-z;U,U)}, \\
C_{zz}^{\mathrm{BR}} &= \frac{d\sigma(r,U;z,U) - d\sigma(r,U;-z,U)}{d\sigma(r,U;z,U) + d\sigma(r,U;-z,U)}, \\
C_{zz}^{\mathrm{TR}} &= \frac{d\sigma(U,z;z,U) - d\sigma(U,z;-z,U)}{d\sigma(U,z;z,U) + d\sigma(U,z;-z,U)}, \\
C_{zz}^{\mathrm{TV}} &= \frac{d\sigma(U,z;U,r) - d\sigma(U,-z;U,r)}{d\sigma(U,z;U,r) + d\sigma(U,-z;U,r)}, \\
C_{zz}^{\mathrm{RV}} &= \frac{d\sigma(U,U;z,r) - d\sigma(U,U;-z,r)}{d\sigma(U,U;z,r) + d\sigma(U,U;-z,r)},
\end{aligned}
\tag{17}
$$

where r denotes the circularly polarized photon beam (the produced vector meson) with helicity $+1$. $\pm z$ stands for the direction of the N (Λ) polarization. The C_{zz}^{BT}, C_{zz}^{BR}, C_{zz}^{TR}, C_{zz}^{TV}, and C_{zz}^{RV} are respectively called the beam-target (BT) asymmetry, the beam-recoil (BR) asymmetry, the target-recoil (TR) asymmetry, the target-vector-meson (TV) asymmetry, and the recoil-vector-meson (RV) asymmetry. We will now see that the effects of the N^* resonances are even more dramatic, particularly in the case of the $\gamma p \to K^{*+}\Lambda$ reaction.

As drawn in the upper panel of Fig. 10, the effects of the N^* resonances on the BT asymmetry for the $\gamma p \to K^{*+}\Lambda$ reaction are prominent in comparison to the results without the N^*. While the C_{zz}^{BT} vanishes at the very backward angle ($\cos\theta = -1$) without the N^* resonances, the inclusion of them brings its value down to be negative (≈ 0.8). It indicates that the polarization of the proton highly depends on the N^* resonances. Interestingly, the effects of the N^* resonances are not at all lessened, even at a higher E_γ. As E_γ increases, the value of the C_{zz}^{BT} turns positive in the forward angle. The effects of the N^* resonances on the neutral process are different from those on the charged one, as depicted in the lower panel of Fig. 10. However, in this case, the BT asymmetry becomes positive in the very backward direction, then turns negative as $\cos\theta$ increases.

The upper and lower panels of Fig. 11 depict the BR asymmetries for the $\gamma p \to K^*\Lambda$ and $\gamma n \to K^{*0}\Lambda$ reactions, respectively. Again, the effects of the N^* resonances on C_{zz}^{BR} are clearly seen in the case of the charged reaction. On the other hand, the N^* effects are marginal for the neutral channel. We come to the same conclusion for the TR, TV,

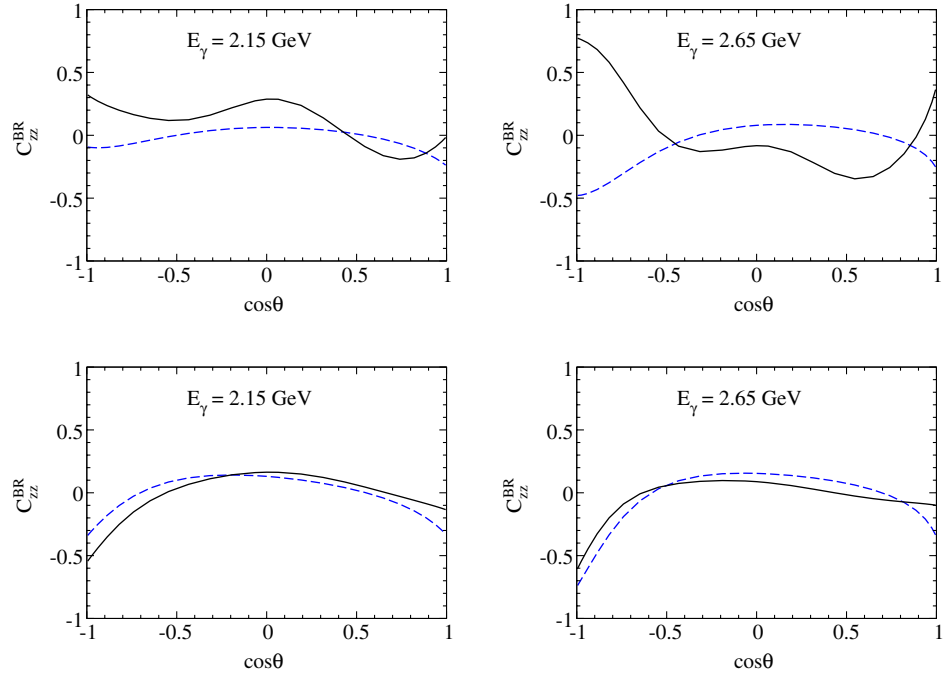

FIG. 11 (color online). The beam-recoil asymmetries as functions of $\cos\theta$ with two different photon energies, $E_\gamma = 2.15$ GeV and $E_\gamma = 2.65$ GeV. In the upper panel, we draw the C_{zz}^{BR} for the $\gamma p \to K^{*+}\Lambda$ reaction, while in the lower panel we do so for the $\gamma n \to K^{*0}\Lambda$ reaction. Notations are the same as in Fig. 7.

and RV asymmetries, as shown in Figs. 12, 13, and 14, respectively. Future measurements of the double polarization observables will be crucial to scrutinizing the role of the N^* resonances in the $\gamma N \to K^*\Lambda$ reactions.

IV. SUMMARY AND CONCLUSION

In the present work, we aimed at investigating the role of the N^* resonances in explaining the production mechanism of $K^*\Lambda$ photoproduction. We included the following N^*

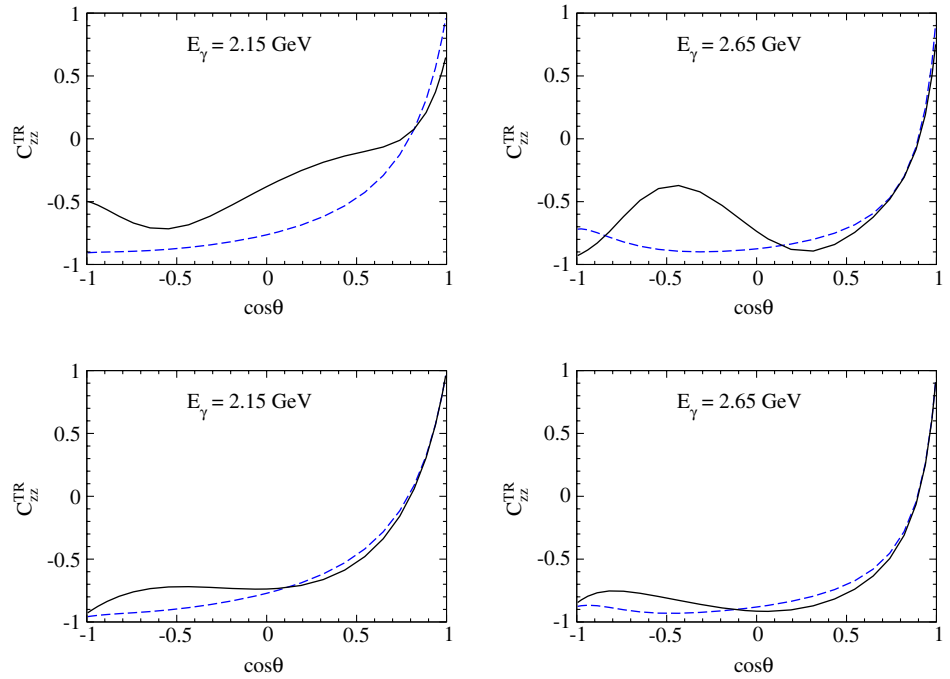

FIG. 12 (color online). The target-recoil asymmetries as functions of $\cos\theta$ with two different photon energies, $E_\gamma = 2.15$ GeV and $E_\gamma = 2.65$ GeV. In the upper panel, we draw the C_{zz}^{TR} for the $\gamma p \to K^{*+}\Lambda$ reaction, while in the lower panel we do so for the $\gamma n \to K^{*0}\Lambda$ reaction. Notations are the same as in Fig. 7.

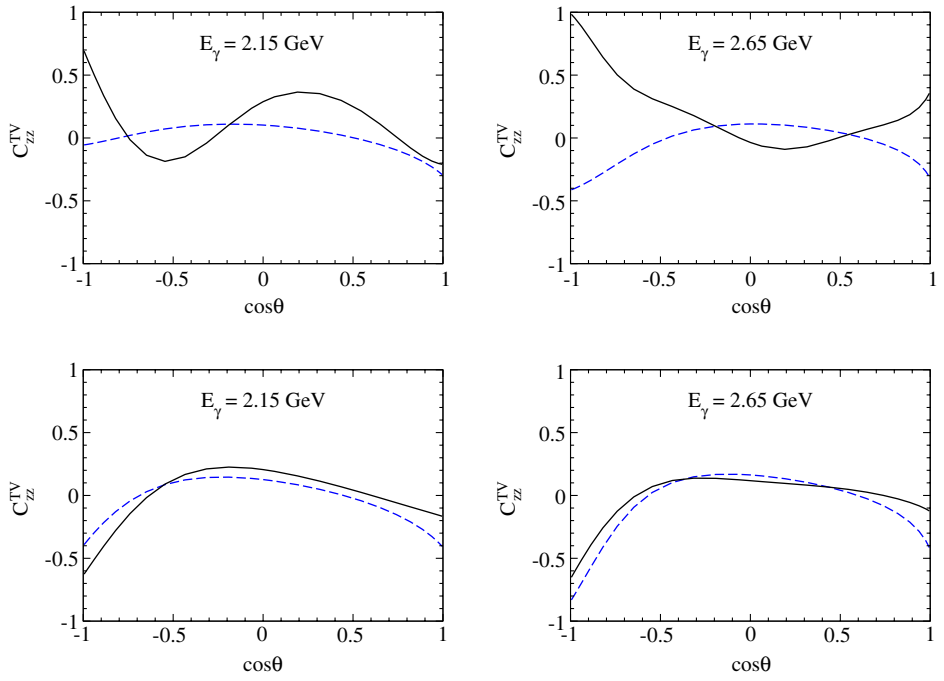

FIG. 13 (color online). The target-vector-meson asymmetries as functions of $\cos\theta$ with two different photon energies, $E_\gamma = 2.15$ GeV and $E_\gamma = 2.65$ GeV. In the upper panel, we draw the C_{zz}^{TV} for the $\gamma p \to K^{*+}\Lambda$ reaction, while in the lower panel we do so for the $\gamma n \to K^{*0}\Lambda$ reaction. Notations are the same as in Fig. 7.

resonances, $N(2000)5/2^+$, $N(2060)5/2^-$, $N(2120)3/2^-$, and $N(2190)7/2^-$ in the vicinity of the threshold, based on the PDG 2012 edition. The coupling constants for the electromagnetic and strong vertices were fixed by the available experimental data or by theoretical predictions. The cutoff masses were determined phenomenologically within a limited range around 1 GeV. The results of the total cross sections were in good agreement with the new CLAS

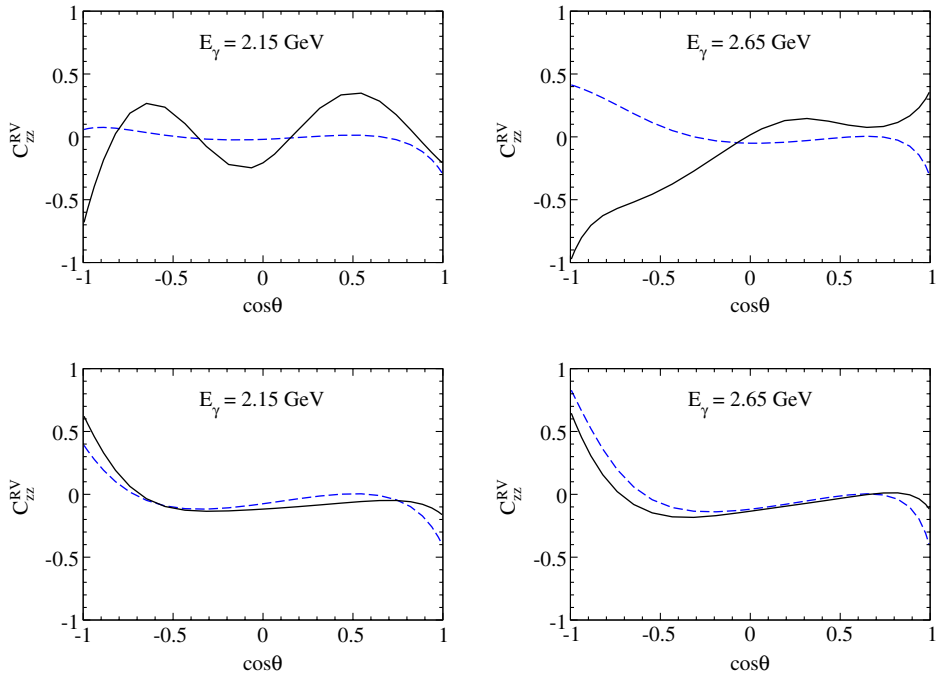

FIG. 14 (color online). The recoil-vector-meson asymmetries as functions of $\cos\theta$ with two different photon energies, $E_\gamma = 2.15$ GeV and $E_\gamma = 2.65$ GeV. In the upper panel, we draw the C_{zz}^{RV} for the $\gamma p \to K^{*+}\Lambda$ reaction, while in the lower panel we do so for the $\gamma n \to K^{*0}\Lambda$ reaction. Notations are the same as in Fig. 7.

data. In particular, the two N^* resonances $N(2120)3/2^-$ and $N(2190)7/2^-$ played very important roles in reproducing the experimental data of the total cross section for the $\gamma p \to K^{*+}\Lambda$ reaction. The differential cross sections were also well described in the range of 1.7 GeV $\leq E_\gamma \leq$ 3.9 GeV, except for the forward angle data in higher photon energies. We predicted the total and differential cross sections for the $\gamma n \to K^{*0}\Lambda$ reaction. It turned out that the N^* resonances come into play in the charged channel, whereas their effects on the neutral channel are marginal. Since the new data for $K^{*0}\Lambda$ photoproduction will soon be reported [37], it will be of great interest to compare the present results with the upcoming CLAS data. We also computed the observables of the single and double polarizations for the $\gamma N \to K^*\Lambda$ reactions. First, the photon-beam asymmetries, the recoil asymmetries, and the target asymmetries were studied. The contribution of the N^* resonances to the single spin asymmetries is prominent in the $\gamma p \to K^{*+}\Lambda$ reaction, while it is less noticeable for $K^{*0}\Lambda$ photoproduction. The five double polarization observables were computed in addition to the single polarization ones, that is, the BT, the BR, the TR, the TV, and the RV asymmetries. We came to the similar conclusion that the N^* resonances govern the angular dependence of the double polarization observables, while their effects are, in general, marginal for the $\gamma n \to K^{*0}\Lambda$ reaction.

As we discussed in the present work, vector-meson photoproduction is especially interesting, since its spin structure has a profound feature coming from the vector meson. We have investigated the effects of the N^* resonances at the Born level in an effective Lagrangian approach, though the N^* resonances turned out to be essential in describing $K^*\Lambda$ photoproduction; other effects might be comparably important—in particular, for the spin observables. For example, the $\gamma N \to K^*\Lambda$ can be regarded as a subprocess of the $\gamma N \to K\pi\Lambda$ reaction. It implies that $K^*\Lambda$ photoproduction may be strongly coupled to another subprocess such as the $\gamma N \to K\Sigma^*(1385)$ reaction. Thus, it is also of great interest to investigate both the $\gamma N \to K^*\Lambda$ and $\gamma N \to K\Sigma^*(1385)$ processes within a coupled-channel formalism. The corresponding investigation is under way.

ACKNOWLEDGMENTS

We are grateful to K. Hicks, W. Tang, and P. Mattione for the invaluable discussion about the new CLAS data. H.-Ch. K. expresses his gratitude to P. Navratil and R. Woloshyn for their hospitality during his visit to TRIUMF, where part of the work was done. S. H. K. is supported by a scholarship from the Ministry of Education, Culture, Science and Technology of Japan. A. H. is supported in part by Grant-in-Aid for Science Research on Priority Areas titled "Elucidation of New Hadrons with a Variety of Flavors" (Grant No. E01:21105006). H.-Ch. K is supported by the Basic Science Research Program through the National Research Foundation of Korea, funded by the Ministry of Education, Science and Technology (Grant No. 2012001083).

[1] W. Tang *et al.* (CLAS Collaboration), Phys. Rev. C **87**, 065204 (2013).
[2] L. Guo and D. P. Weygand (CLAS Collaboration), arXiv: hep-ex/0601010.
[3] S. H. Kim, S. i. Nam, Y. Oh, and H.-Ch. Kim, Phys. Rev. D **84**, 114023 (2011).
[4] Y. Oh and H. Kim, Phys. Rev. C **73**, 065202 (2006).
[5] Y. Oh and H. Kim, Phys. Rev. C **74**, 015208 (2006).
[6] S. Ozaki, H. Nagahiro, and A. Hosaka, Phys. Rev. C **81**, 035206 (2010).
[7] J. Beringer *et al.* (Particle Data Group), Phys. Rev. D **86**, 010001 (2012).
[8] K. Nakamura *et al.* (Particle Data Group), J. Phys. G: Nucl. Part. Phys. **37**, 075021 (2010).
[9] A. V. Anisovich, R. Beck, E. Klempt, V. A. Nikonov, A. V. Sarantsev, and U. Thoma, Eur. Phys. J. A **48**, 15 (2012).
[10] G. Höhler, F. Kaiser, R. Koch, and E. Pietarinen, *Handbook of Pion Nucleon Scattering*, Physics Data, No. 12-1 (Fachinformationszentrum, Karlsruhe, 1979).
[11] A. V. Anisovich, E. Klempt, V. A. Nikonov, A. V. Sarantsev, H. Schmieden, and U. Thoma, Phys. Lett. B **711**, 162 (2012).
[12] A. V. Anisovich, E. Klempt, V. A. Nikonov, A. V. Sarantsev, and U. Thoma, Phys. Lett. B **711**, 167 (2012).
[13] N. Awaji, H. Hayashii, S. Iwata, R. Kajikawa, K. Makino, A. Miyamoto, H. Ozaki, A. Sugiyama *et al.*, *Proceedings for 10th International Symposium on Lepton and Photon Interactions at High Energy*, edited by W. P. Bonn (Bonn University, Physics Institute, Germany, 1981), p. 1056.
[14] K. Fujii, H. Hayashii, S. Iwata, R. Kajikawa, A. Miyamoto, T. Nakanishi, Y. Ohashi, S. Okumi *et al.*, Nucl. Phys. **B197**, 365 (1982).
[15] D. Black, M. Harada, and J. Schechter, Phys. Rev. Lett. **88**, 181603 (2002).
[16] W. Rarita and J. Schwinger, Phys. Rev. **60**, 61 (1941).
[17] B. J. Read, Nucl. Phys. **B52**, 565 (1973).
[18] Th. A. Rijken, V. G. J. Stoks, and Y. Yamamoto, Phys. Rev. C **59**, 21 (1999).
[19] S.-J. Chang, Phys. Rev. **161**, 1308 (1967).
[20] J. G. Rushbrooke, Phys. Rev. **143**, 1345 (1966).
[21] R. E. Behrends and C. Fronsdal, Phys. Rev. **106**, 345 (1957).
[22] Y. Oh, EPJ Web Conf. **20**, 02008 (2012).

[23] S. i. Nam, A. Hosaka, and H.-Ch. Kim, Phys. Rev. D **71**, 114012 (2005).
[24] A. V. Anisovich, R. Beck, E. Klempt, V. A. Nikonov, A. V. Sarantsev, and U. Thoma, Eur. Phys. J. A **49**, 67 (2013).
[25] S. Capstick, Phys. Rev. D **46**, 2864 (1992).
[26] S. Capstick and W. Roberts, Phys. Rev. D **58**, 074011 (1998).
[27] M. Chretien and R. E. Peierls, Proc. R. Soc. A **223**, 468 (1954).
[28] H. Haberzettl, C. Bennhold, T. Mart, and T. Feuster, Phys. Rev. C **58**, R40 (1998).
[29] R. M. Davidson and R. Workman, Phys. Rev. C **63**, 025210 (2001).
[30] H. Haberzettl, K. Nakayama, and S. Krewald, Phys. Rev. C **74**, 045202 (2006).
[31] K. Hicks, D. Keller, and W. Tang, AIP Conf. Proc. **1374**, 177 (2011).
[32] S. H. Kim, S. i. Nam, A. Hosaka, and H.-Ch. Kim, Phys. Rev. D **88**, 054012 (2013).
[33] S. H. Kim, S. i. Nam, A. Hosaka, and H.-Ch. Kim, arXiv:1310.6551.
[34] C. G. Fasano, F. Tabakin, and B. Saghai, Phys. Rev. C **46**, 2430 (1992).
[35] M. Pichowsky, C. Savkli, and F. Tabakin, Phys. Rev. C **53**, 593 (1996).
[36] A. I. Titov, Y. Oh, S. N. Yang, and T. Morii, Phys. Rev. C **58**, 2429 (1998).
[37] P. Mattione (private communication).